Southern Ocean Ventilation Links the Drake Passage to the Atlantic Meridional Overturning Circulation

Zhanghanshu Han[a], Haijun Yang*[a], Mingjun Tong[a], Xiaoming Hu[b]

[a] *Department of Atmospheric and Oceanic Sciences, Institute of Atmospheric Sciences, and Key Laboratory of Polar Atmosphere-Ocean-Ice System for Weather and Climate of Ministry of Education, Fudan University, Shanghai 200438, China*

[b] *School of Atmospheric Sciences, Sun Yat-sen University and Southern Marine Science and Engineering Guangdong Laboratory (Zhuhai), Zhuhai 519082, China*

TBD

September 21, 2026

Submitted

**Corresponding author*: Haijun Yang, yanghj@fudan.edu.cn

ABSTRACT

The Drake Passage (DP) provides the only deep circumpolar connection around Antarctica and is therefore central to Southern Ocean circulation and global deep-ocean ventilation. Here, using a fully coupled climate model, we investigate how the Atlantic Meridional Overturning Circulation (AMOC) adjusts to the closure and subsequent reopening of the DP. Closing the DP blocks the Antarctic Circumpolar Current (ACC) and reorganizes both atmospheric and oceanic circulations around Antarctica. Antarctic warming and sea-ice retreat alter surface buoyancy forcing, while a weakened meridional temperature gradient reduces the Southern Hemisphere westerlies and develops an anomalous high-pressure and anticyclonic circulation over the Ross Sea. This leads to weaker Southern Ocean Ekman upwelling but enhanced downwelling and deep convection in the Ross Sea, strongly enhancing Antarctic Bottom Water (AABW) formation there. The resulting AABW-dominated abyssal circulation occupies the deep return pathway and disconnects North Atlantic Deep Water (NADW) from its principal upwelling branch in the Southern Ocean, leading to the gradual collapse of the NADW-dominated AMOC. When the DP is reopened, the ACC and Southern Ocean Ekman upwelling recover rapidly, AABW weakens, and the AMOC is subsequently reestablished on a longer adjustment timescale. These results show that the influence of the DP on the AMOC is mediated primarily through the reorganization of Southern Ocean ventilation, involving both wind-driven upwelling and AABW-controlled abyssal pathways.

KEYWORDS: Drake Passage; Atlantic Meridional Overturning Circulation; Antarctic Bottom Water; Southern Ocean upwelling; CESM1

1. Introduction

The Drake Passage (DP), located between the southern tip of South America and the Antarctic Peninsula, is the only deep gateway connecting the major ocean basins around Antarctica. Its opening was a prolonged tectonic process that began during the Cenozoic and ultimately permitted the establishment of an unblocked circumpolar pathway around Antarctica (Zachos et al. 2001; Scher and Martin 2006; Lagabrielle et al. 2009). This gateway is a prerequisite for the Antarctic Circumpolar Current (ACC), which connects the Atlantic, Pacific, and Indian Oceans and enables large-scale exchanges of heat, salt, and water masses among the major basins (Chidichimo et al. 2014; Koenig et al. 2014; Donohue et al. 2016; Xu et al. 2020; Gutierrez-Villanueva et al. 2023). Driven by strong Southern Hemisphere westerlies and maintained by steep meridional density gradients, the ACC is the largest zonal current in the global ocean, with transport through the DP exceeding 140 Sv in modern observations. By regulating both circumpolar exchange and Southern Ocean overturning, the DP constitutes a key geographic control on the global ocean circulation.

A large body of modeling work (Table 1) has shown that changes in the DP can substantially reorganize both Southern Ocean circulation and the Atlantic Meridional Overturning Circulation (AMOC) (Mikolajewicz et al. 1993; Toggweiler and Samuels 1995; Toggweiler and Bjornsson 2000; Nong et al. 2000; Sijp and England 2004, 2005, 2009; Sijp et al. 2009; Hutchinson et al. 2013; Yang et al. 2014; England et al. 2017; Toumoulin et al. 2020). When the DP is open, strong Southern Hemisphere westerlies drive northward Ekman transport and upwelling in the Southern Ocean, providing an important return pathway for North Atlantic Deep Water (NADW). Closing the DP blocks the ACC and reorganizes the Southern Ocean into closed gyre circulations, thereby weakening both wind-driven upwelling and NADW. Previous studies generally show that DP closure enhances Antarctic Bottom Water (AABW) formation and strengthens the abyssal overturning circulation, allowing AABW to expand northward into the Atlantic and Pacific basins (Mikolajewicz et al. 1993; Sijp and England 2004, 2005, 2009; Sijp et al. 2009; Hutchinson et al. 2013; Yang et al. 2014; England et al. 2017; Toumoulin et al. 2020). The response of the AMOC can therefore be viewed in terms of the competition between NADW and AABW for deep-ocean ventilation, particularly for access to the Southern Ocean upwelling branch that closes the global overturning circulation.

TABLE 1. List of past modeling studies on the effect of the DP on ocean circulation and global climate.

Authors	Model	Atmosphere	Bathymetry	pCO2

Mikolajewicz et al. (1993)	Hamburg	None	Modern	None
Toggweiler and Samuels (1995)	MOM1	None	Modern	None
Toggweiler and Bjornsson (2000)	MOM2	EBMa	Aquaplanet	280 ppm
Nong et al. (2000)	CSM	None	Modern	None
Sijp and England (2004)	Uvic	EBM	Modern	280 ppm
Sijp and England (2005)	Uvic	EBM	Modern	280 ppm
Sijp and England (2009)	Uvic	EBM	Modern	280 ppm
Sijp et al. (2009)	Uvic	EBM	Modern	280, 500, 750, 1000, 1250, 1500, 1750, 2000 ppm
Sijp et al. (2011)	Uvic	EBM	Eocene	1500 ppm
Zhang et al. (2010)	FOAM	CCM2	Eocene	2240 ppm
Zhang et al. (2011)	FOAM	CCM2	Eocene	2240 ppm
Cristini et al. (2012)	COSMOS	ECHAM5.4	Eocene	280 ppm
Lefebvre et al. (2012)	FOAM	CCM2	Eocene	280, 420, 560, 700, 840 ppm
Hutchinson et al. (2013)	CSIRO-Mk3L	Mk3L	Modern	A2c, 856 ppm
Hill et al. (2013)	HadCM3L	HadCM3L	Oligocene	560 ppm
Yang et al. (2014)	CM2MC	AM2	Modern	280 ppm
Pfister et al. (2014)	Bern3D	EBM	Modernb	280 ppm
Goldner et al. (2014)	CESM1.0	CAM4	Eocene	1120 ppm
Fyke et al. (2015)	Uvic	EBM	Modern	560, 840, 1120, 1400 ppm
Viebahn et al. (2016)	POP	None	Modern	None
England et al. (2017)	CSIRO-Mk3L	Mk3L	Modern	280 ppm
Elsworth et al. (2017)	CM2MC	AM2	Modernb	280 ppm
Ladant et al. (2018)	IPSL-CM5A	LMDz	Modernb	1120 ppm

Hutchinson et al. (2018)	CM2.1	AM2	Eocene	400, 800, 1600 ppm
Kennedy-Asser et al. (2019)	HadCM3BL	HadCM3L	Oligocene	560, 840, 1120 ppm
Toumoulin et al. (2020)	IPSL-CM5A2	LMDz	Eocene	1120 ppm
Wang et al. (2024, 2025)	CESM1.2.2	CAM4	Modern	370, 740 ppm

[a] Energy Balance Model

[b] Panama Seaway open

[c] High-emission scenario (Nakicenovic and Swart 2000)

The climatic significance of the DP has also been widely discussed in a paleoclimate context. Because the opening of the DP, the establishment of the ACC, and the major Antarctic cooling associated with the Eocene–Oligocene transition occurred within broadly overlapping geological intervals, early studies proposed that the opening of the passage may have contributed to Antarctic cooling by thermally isolating the continent and reorganizing the global overturning circulation (Jamieson et al. 2010, 2023). Under modern boundary conditions, several early modeling studies further suggested that the DP could exert a strong control on the existence of NADW, with closure of the passage leading to a severe weakening or shutdown of the AMOC (Mikolajewicz et al. 1993; Toggweiler and Samuels 1995; Toggweiler and Bjornsson 2000; Nong et al. 2000; Sijp and England 2004, 2005; Sijp et al. 2009). A broad survey of these modeling efforts (Table 1) indicates that the early studies predominantly used simplified ocean models or energy-balance atmospheres, while later fully coupled General Circulation Model (GCM) produced more diverse responses depending on model complexity. Later studies, however, showed that the AMOC response to DP closure is sensitive to the representation of coupled climate processes, including atmospheric moisture transport, vertical mixing, and sea-ice feedbacks (Sijp and England 2009; Hutchinson et al. 2013; Yang et al. 2014; England et al. 2017). Likewise, interpretations of Antarctic glaciation at the Eocene–Oligocene transition have increasingly emphasized the combined effects of atmospheric CO_2, paleogeography, ice–albedo feedbacks, and ocean gateway changes rather than a singular control by the DP (DeConto and Pollard 2003; Zhang et al. 2010, 2011; Sijp et al. 2011; Cristini et al. 2012; Lefebvre et al. 2012; Hill et al. 2013; Goldner et al. 2014; Hutchinson et al. 2018; Kennedy-Asser et al. 2019; Toumoulin et al. 2020). Moreover, many of these GCM-based paleoclimate experiments (Table 1) were carried out under drastically different boundary conditions (e.g., Eocene geography and elevated CO_2), making it difficult to directly isolate the pure dynamical effect of the DP under modern settings. These studies establish that the DP can strongly influence the coupled climate system, but they also indicate that the pathway linking gateway geometry to AMOC adjustment is not universal and depends on how Southern Ocean processes are represented.

Despite extensive previous work, most studies have focused on equilibrium differences between open- and closed-DP configurations, while the transient adjustment of the coupled atmosphere–ocean system between these states has received much less attention. An important exception is England et al. (2017), who showed that DP closure can initially strengthen AABW sufficiently to suppress NADW, followed by a later recovery of the AMOC as sea-ice feedbacks weaken AABW formation. However, how the Southern Ocean circulation, atmospheric forcing, deep-water formation, and AMOC co-evolve during both DP closure and reopening remains incompletely understood. The sequential closure–reopening experiments designed in this study are intended to fill this gap by tracking the full transient evolution and isolating the underlying mechanisms.

Our previous coupled-model studies have shown that large-scale topographic features, including the Tibetan Plateau and Antarctica, play a fundamental role in shaping the modern global meridional overturning circulation (Yang and Wen 2020; Wen and Yang 2020; Jiang and Yang 2021; Yang et al. 2024; Tong et al. 2025), and that DP-induced circulation changes can substantially affect tropical climate variability (Han et al. 2026). Here, we extend this framework by performing sequential experiments in which the DP is first closed and then reopened in a fully coupled climate model. This experimental design allows us to track the transient evolution and reversibility of the overturning circulation and to isolate the processes connecting DP geometry to AMOC collapse and recovery. We show that the key adjustment occurs through a reorganization of Southern Ocean ventilation: DP closure enhances AABW formation by warming Antarctica and altering the ocean and atmospheric circulations over the Ross Sea, while weakening wind-driven Southern Ocean upwelling, thereby disrupting the deep return pathway of NADW and leading to AMOC collapse; reopening the passage reverses these processes and permits the AMOC to recover.

The remainder of the paper is organized as follows. Section 2 describes the model and experimental design. Section 3 documents the AMOC response to DP closure and reopening. Section 4 examines the associated oceanic and atmospheric mechanisms. Section 5 summarizes the main conclusions and discusses their broader implications.

2. Model and Experiments

a. Model

We use version 1.0.4 of the Community Earth System Model (CESM1), developed by the National Center for Atmospheric Research (NCAR). CESM1 is a fully coupled climate model that has been widely used for both modern and paleoclimate simulations. Its ocean component, the Parallel Ocean Program version 2 (POP2), has been extensively evaluated for its representation of the AMOC, ACC, Deacon cell, and other aspects of Southern Ocean circulation (Russell et al. 2006; Sen Gupta et al. 2009; Farneti et al. 2015; Beadling et al. 2019, 2020; Tsujino et al. 2020; Weijer et al. 2020; Gong et al. 2022).

The model configuration used here is T31_gx3v7 and includes interactive atmosphere, ocean, sea ice, land, and coupler components. The atmospheric component is the Community Atmosphere Model version 4 (CAM4), with a horizontal resolution of approximately 3.75° × 3.75° and 26 vertical levels. The ocean component, POP2, has a uniform zonal grid spacing of 3.6° and a nonuniform meridional grid, with the meridional resolution ranging from approximately 3.4° near 35°N and 35°S to about 0.6° near the equator. POP2 includes 60 vertical levels. The sea ice component, CICE4, uses the same horizontal grid as POP2. Further details of CESM1 are provided by Hurrell et al. (2013).

b. Experiments

We conduct a sequence of three fully coupled experiments to examine the transient response of the climate system to the closure and reopening of the DP. The control experiment, referred to as Real, is integrated for 800 years (years 1–800) using realistic modern topography. At year 801, the DP is closed by introducing an isthmus approximately 500 km wide between the Antarctic Peninsula and Cape Horn, South America. This experiment, referred to as DPC, is then integrated for another 800 years (years 801–1600). At year 1601, the DP is reopened by restoring the original topography, and the model is integrated for a further 800 years (years 1601–2400) in the DPO experiment.

The imposed DP closure follows the idealized configuration commonly used in previous gateway studies (Mikolajewicz et al. 1993; Sijp and England 2004, 2005, 2009; Sijp et al. 2009; Hutchinson et al. 2013; Yang et al. 2014; England et al. 2017; Wang et al. 2024, 2025; Han et al.

2026). Apart from the prescribed topographic change at the DP, all model components, resolutions, external forcing, and boundary conditions are kept identical among the experiments and remain fixed at preindustrial settings. This sequential design allows us to diagnose both the adjustment toward the closed-DP state and the reversibility of the circulation response after the passage is reopened.

c. Overturning indices

Several indices are defined to characterize the strength of the meridional overturning circulation. The M55 index is defined as the minimum (negative) value of the meridional overturning streamfunction in the region from 55°S to 80°S and from the surface to 4000 m depth, representing the strength of AABW formation. The M30 index is defined as the minimum (negative) value of the overturning streamfunction north of 30°S and between 2600 and 5000 m depth, representing the strength of the abyssal overturning circulation dominated by AABW (Wen et al. 2021). The AMOC index is defined as the maximum value of the Atlantic meridional overturning streamfunction below 500 m depth between 20°N and 70°N, representing the strength of the NADW-dominated upper overturning cell. For comparison, the Pacific meridional overturning circulation (PMOC) index is defined as the maximum value of the meridional overturning streamfunction below 500 m depth between 20°N and 70°N in the Pacific. All index time series are smoothed using a 10-year running mean to suppress high-frequency interannual variability.

3. Effect of DP closure and reopening on the AMOC

The closure of the DP produces an immediate and pronounced response in AABW formation and the associated abyssal overturning circulation. Within the first decade after closure, AABW formation strengthens rapidly, with M55 exceeding 40 Sv, while the deep overturning circulation represented by M30 exceeds 30 Sv (Figs. 1a, b). This initial intensification is consistent with previous studies showing a strong enhancement of AABW following DP closure (Mikolajewicz et al. 1993; Sijp and England 2004, 2005; England et al. 2017). After approximately 10 years, however, M55 decreases to about 30 Sv and remains relatively stable throughout the remainder of the closed-DP experiment. In contrast, M30 rapidly returns toward its control-state value and subsequently strengthens modestly by approximately 6 Sv. When the DP is reopened, M55 decreases abruptly to below 20 Sv, while M30 also weakens gradually; both indices ultimately recover toward their values in the Real experiment.

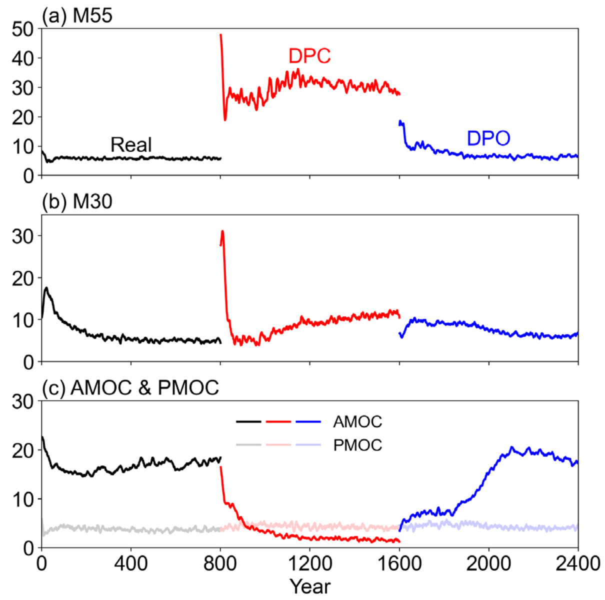

FIG. 1. Time series of (a) M55, (b) M30, and (c) the AMOC and PMOC indices (units: Sv) for the three experiments: Real (years 1–800; black), DPC (years 801–1600; red), and DPO (years 1601–2400; blue).

The AMOC responds much more slowly than AABW to DP closure. Its strength declines substantially during the first century, and NADW formation is nearly absent by around year 1200. The recovery is similarly slow: following DP reopening, the AMOC requires more than 500 years to return toward its control-state strength (Fig. 1c). Thus, compared with the rapid adjustment of AABW, the AMOC exhibits a markedly longer response timescale to both closure and reopening of the DP. In contrast, the PMOC remains at a consistently low level throughout the experiments, showing little change (Fig. 1c).

The spatial evolution of the overturning circulation reveals how this transition occurs (Fig. 2). AABW strengthens almost immediately after closure and rapidly expands northward into both the Atlantic and Pacific basins, while the Deacon cell shoals markedly from its control-state depth of about 3000 m to roughly 500 m (Figs. 2a2–c2). During the first decade, however, NADW formation remains vigorous and continues to occupy the upper ~3000 m of the North Atlantic. At the same time, the strengthened AABW-dominated abyssal circulation increasingly occupies the deep Southern Ocean and disrupts the usual connection between NADW and Southern Ocean upwelling. With this high-latitude return pathway restricted, NADW is forced to return toward the surface farther north, primarily through weak low-latitude upwelling (Figs. 2a2). As the adjustment proceeds, AABW weakens from its initial peak and temporarily retreats from parts of the Atlantic (Fig. 2a4), but the deep Southern Ocean remains dominated by the AABW-associated circulation below about 500 m (Fig. 2c4). Consequently, the principal Southern Ocean return pathway for NADW remains strongly constrained and the AMOC does not recover (Figs. 2a5, a6). NADW formation ultimately shuts down, after which AABW again dominates the deep Atlantic circulation (Figs. 2a5, a6). The overturning structure approaches a quasi-equilibrium closed-DP state after roughly 200 years (Figs. 2a5, a6). Enhanced AABW enters not only the Atlantic basin but also the Pacific basin, strengthening the deep circulation (Figs. 2b2–b6).

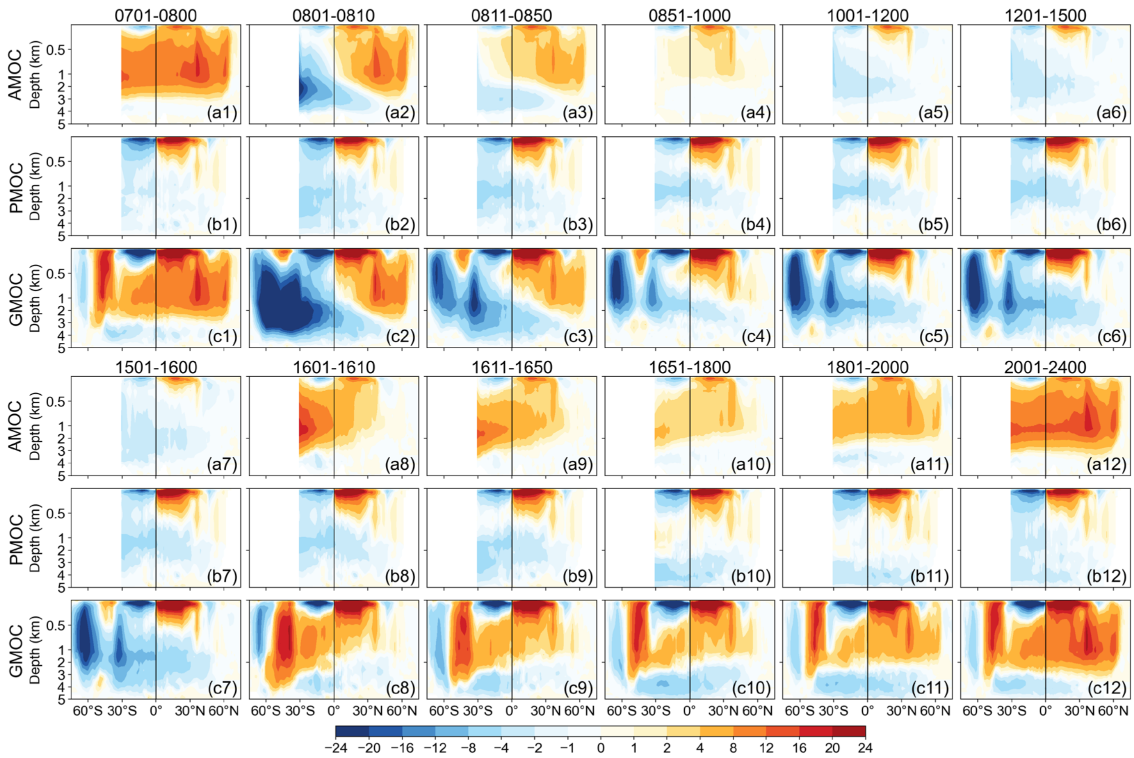

FIG. 2. Patterns of (a) the AMOC, (b) the PMOC, and (c) the global MOC (GMOC) averaged over the years indicated in the figure (units: Sv).

After the DP is reopened, AABW formation weakens abruptly (Fig. 1a), and the AABW-dominated abyssal circulation can no longer be maintained. The Southern Ocean overturning reverses rapidly toward its control-state configuration (Fig. 2c7), before the coupled atmosphere–ocean system has fully adjusted. This emerging upwelling branch expands northward into the Atlantic and progressively reconnects with the upper-ocean circulation (Figs. 2a8–a10). At the same time, the wind-driven Deacon cell recovers quickly in both strength and vertical extent (Figs. 2c8–c10). Notably, Southern Ocean upwelling is largely reestablished by years 1651–1800 (Fig. 2c10), whereas the NADW-dominated AMOC remains substantially weaker than in the Real experiment (Fig. 2a10). Thus, the Southern Ocean return pathway recovers on a shorter timescale than NADW formation itself. During this interval, a weak Pacific overturning cell develops temporarily (Fig. 2b10), providing part of the compensating downwelling required to balance the restored Southern Ocean upwelling (Gnanadesikan 1999; Johnson et al. 2007; Baker et al. 2025). As the North Atlantic circulation continues to adjust, NADW strengthens and progressively assumes the dominant role in balancing the Southern Ocean upwelling.

Once Southern Ocean upwelling has been reestablished, the remaining adjustment occurs primarily in the North Atlantic. Because the background conditions favorable for NADW formation are retained in these experiments (Ferreira et al. 2018; Yang and Wen 2020; Yang et al. 2024; Tong et al. 2025), the AMOC gradually strengthens as its large-scale overturning structure reconnects with the recovered Southern Ocean upwelling branch (Figs. 2a11). This recovery is further reinforced by the sea ice–salinity feedback in the North Atlantic (Stommel 1961; Brady and Otto-Bliesner 2011; Yang and Wen 2020), allowing both the AMOC strength (Fig. 1c) and spatial structure to return toward their Real-state values. The adjustment following DP closure and reopening is therefore strongly asymmetric in time: AABW and the Southern Ocean overturning respond rapidly to changes in gateway geometry, whereas the NADW-dominated AMOC adjusts over several centuries. Nevertheless, under the opposing topographic perturbations applied here, the coupled overturning circulation ultimately returns close to its initial state, indicating that the large-scale response is approximately reversible.

4. Mechanisms

a. Changes in ocean temperature, salinity and density

The meridional overturning circulation is tightly coupled to the large-scale distributions of ocean temperature, salinity, and density (Stommel 1961; Rahmstorf 2002; Cai et al. 2023). Fig. 3 shows the evolution of the global zonal-mean temperature, salinity, and density fields at selected times after DP closure and reopening. Following DP closure, the loss of an unblocked circumpolar pathway allows the reorganized Southern Ocean circulation to transport more subtropical warm water toward Antarctica, producing pronounced warming in the upper ~1000 m of the Southern

Ocean, with the largest anomalies near the surface (Figs. 3a1–a4). At the same time, the shutdown of the NADW-dominated AMOC reduces the northward warm water transport in the North Atlantic, leading to marked cooling at high northern latitudes and widespread cooling of the deep ocean (Fig. a4). The Southern Ocean also becomes substantially saltier above ~1000 m (Figs. 3b1–b4), consistent with enhanced poleward transport of saline subtropical waters and strengthened AABW formation. In contrast, the high-latitude North Atlantic freshens strongly, with the freshening extending to depths of nearly 3000 m as NADW formation weakens (Fig. b4). A secondary salinity increase develops in the tropical Northern Hemisphere, likely reflecting reduced precipitation associated with the southward displacement of the Intertropical Convergence Zone (ITCZ) following the AMOC collapse (Broccoli et al. 2006; Yang et al. 2014; Liu and Hu 2015; Kug et al. 2021; Kim et al. 2023; Oh et al. 2024; Han et al. 2026).

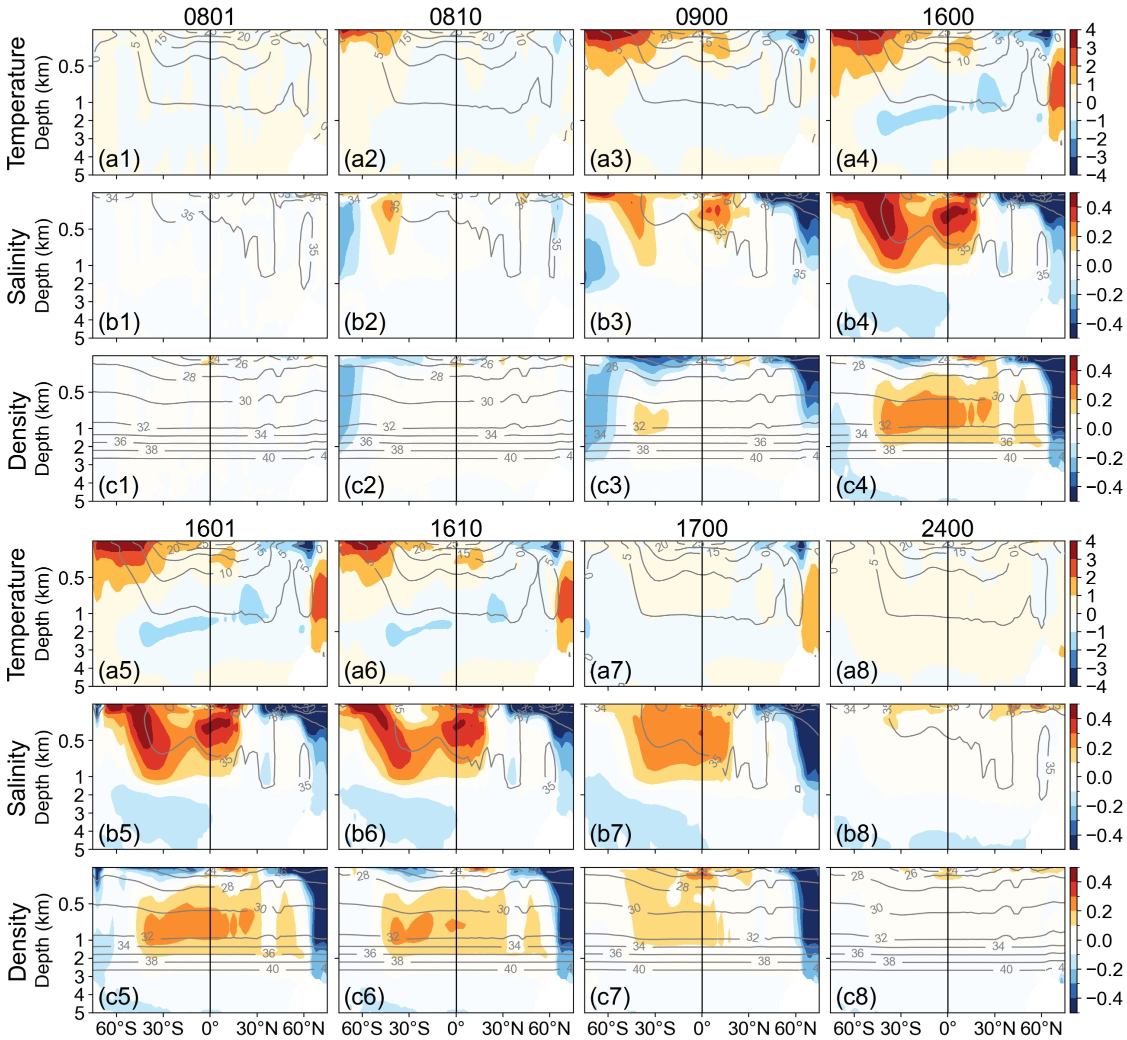

FIG. 3. Global zonal mean sections of (a) temperature (units: °C), (b) salinity (units: psu), and (c) density (units: kg m^{-3}) at years 1, 10, 100, and 800 after the DP closure and reopening, with the years

indicated in the figure. Shading denotes changes relative to the 701–800 mean, and contours denote the mean values for the corresponding years.

Although the upper ~1000 m in the Southern Ocean becomes warmer and saltier after DP closure, the deeper ocean there becomes colder and fresher. These opposing changes substantially modify the vertical density structure. Surface density decreases in the upper few hundred meters, while density increases at intermediate depths of roughly 400–3000 m, resulting in stronger stratification (Fig. 3c4). The accompanying flattening of isopycnals and poleward displacement of their surface outcrops reduce the ability of deep waters to access the surface in the Southern Ocean, thereby suppressing the upwelling branch of the overturning circulation (Stommel 1958; Munk 1966; Marshall and Speer 2012; Watson et al. 2013; Cai et al. 2023). In this sense, the AABW-dominated deep circulation is associated not only with a replacement of NADW in the abyssal ocean but also with a more strongly stratified Southern Ocean that further restricts deep-water return to the surface. After the DP is reopened, these temperature, salinity, and density anomalies gradually diminish and the large-scale hydrographic structure returns toward its Real-state configuration (Figs. 3a5–c8).

The surface fields provide a clearer view of the regional expression of this hydrographic adjustment (Fig. 4). Following DP closure, pronounced SST warming develops throughout the Southern Ocean, with particularly large anomalies in the subpolar South Pacific and along the Antarctic margin (Figs. 4a1–a3). This pattern is consistent with the reorganized Southern Ocean circulation, which permits greater poleward transport of relatively warm subtropical waters into the Bellingshausen and Ross Seas. Sea surface salinity also increases over much of the Southern Ocean, with strong positive anomalies extending into the Bellingshausen and Ross Seas (Figs. 4b1–b3). In contrast, the subpolar North Atlantic becomes substantially fresher as the AMOC weakens and northward salt transport declines. Despite the concurrent warming and salinification around Antarctica, the thermal contribution dominates the surface density response over much of the Southern Ocean, producing widespread negative sea surface density anomalies (Figs. 4c1–c3). In contrast, the saline contribution dominates the surface density response in the North Atlantic.

Positive density anomalies are confined mainly to parts of the tropical Northern Hemisphere, where the salinity increase is sufficiently strong to offset the temperature effect. Thus, the surface response to DP closure is characterized by a warm, saline, but generally lighter Southern Ocean surface layer, consistent with the strengthened upper-ocean stratification identified in Fig. 3. After the DP is reopened, these surface anomalies largely reverse and gradually return toward the Real-state distributions (Figs. 4a4–c5). In particular, the Southern Ocean anomalies recover largely within the second century after reopening, with temperature anomalies nearly returning to the control level as early as the first century (Figs. 3a7, 4a4).

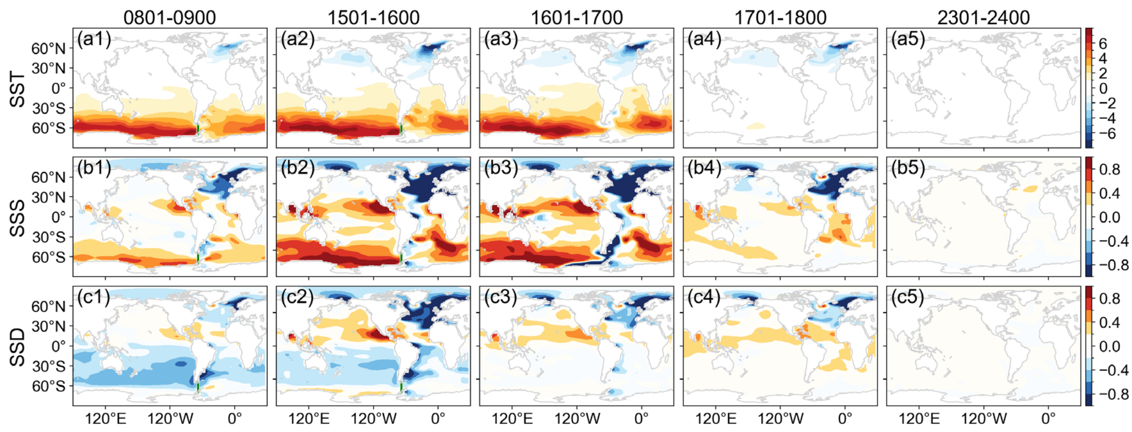

FIG. 4. Changes in (a) sea surface temperature (SST; units: °C), (b) sea surface salinity (SSS; units: psu), and (c) sea surface density (SSD; units: kg m^{-3}) relative to the 701–800 mean, with the years indicated in the figure, corresponding to the first and last 100 years after DP closure and reopening, respectively.

b. Changes in atmospheric forcing and ocean circulation

The rapid enhancement of AABW following DP closure is central to the subsequent reorganization of the Southern Ocean overturning and the collapse of the AMOC. Yet this enhancement occurs despite substantial surface warming in the principal AABW source regions, even with winter sea ice in the control state disappearing, particularly in the Ross Sea (Figs. 4a1–a3), indicating that temperature alone cannot explain the deep-convection response. We therefore examine changes in surface buoyancy forcing during austral winter, when AABW formation is most active (Marshall and Schott 1999; Orsi et al. 1999; Wen et al. 2021). The surface buoyancy flux is separated into thermal and haline components, which exert competing influences on upper-ocean density and convection. Following DP closure, winter sea ice retreats markedly around Antarctica, especially in the Bellingshausen and Ross Seas. The newly exposed ocean surface experiences enhanced wintertime heat loss, producing a substantial reduction in thermal buoyancy input and thus favoring surface densification and deep convection (Figs. 5a1, a2).

The haline response acts in the opposite direction. Sea-ice retreat and enhanced melting increase freshwater input to the exposed ocean surface, while reduced sea-ice formation weakens brine rejection. These changes increase the haline buoyancy input in the Bellingshausen and Ross Seas (Figs. 5b1, b2) and therefore tend to suppress AABW formation, consistent with the mechanism emphasized by England et al. (2017). In the present experiments, however, this stabilizing haline effect is more than offset by the enhanced thermal buoyancy loss, so that the net surface buoyancy flux decreases substantially over the Bellingshausen and Ross Seas (Figs. 5c1, c2). At the same time, the reorganized Southern Ocean circulation transports relatively saline subtropical water poleward into these regions (Figs. 4b1–b3), helping maintain sufficiently high surface salinity despite weaker brine rejection. The combined effect is therefore an increase in surface-water density and convective potential in key AABW source regions, particularly the Ross Sea. In contrast, changes in the Weddell Sea are comparatively weak.

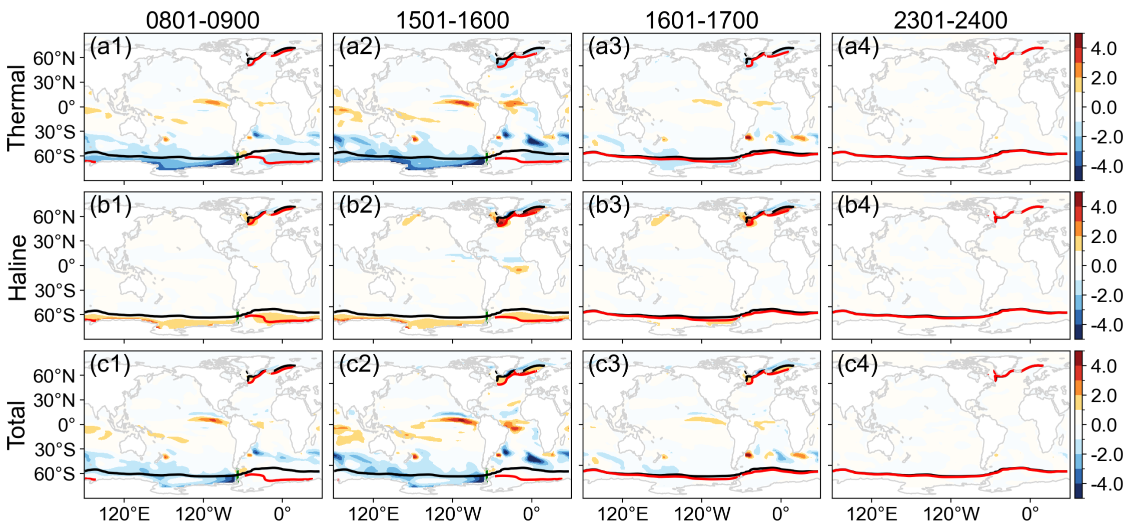

FIG. 5. Changes in (a) thermal buoyancy flux (units: 10^{-8} m^2 s^{-3}), (b) haline buoyancy flux (units: 10^{-8} m^2 s^{-3}), and (c) total buoyancy flux (units: 10^{-8} m^2 s^{-3}) during the austral winter, relative to the 701–800 mean. In (a) and (b), positive values indicate that the ocean gains heat and fresh water from the atmosphere. The black curve denotes the 701–800 mean sea ice edge, and the red curve denotes the sea ice edge at the corresponding time, defined as 15% sea ice concentration. Areas without contours indicate no sea ice, with the years indicated in the figure.

In fact, DP closure substantially alters the atmospheric circulation over the Southern Ocean. The pronounced Southern Ocean warming associated with the loss of the circumpolar pathway reduces the meridional temperature gradient between Antarctica and the Southern Hemisphere midlatitudes. Consistent with thermal-wind balance, the midlatitude westerlies weaken markedly (Fig. 6a), resembling a shift toward the negative phase of the Southern Annular Mode (SAM) (England et al. 2017). The atmospheric response is accompanied by increased sea level pressure over Antarctica and the adjacent high-latitude Southern Ocean and decreased pressure farther equatorward, with the strongest anomalies occurring over the South Pacific and Ross Sea sector (Figs. 7a1–a2). These pressure changes support an anomalous anticyclonic circulation over the Ross Sea.

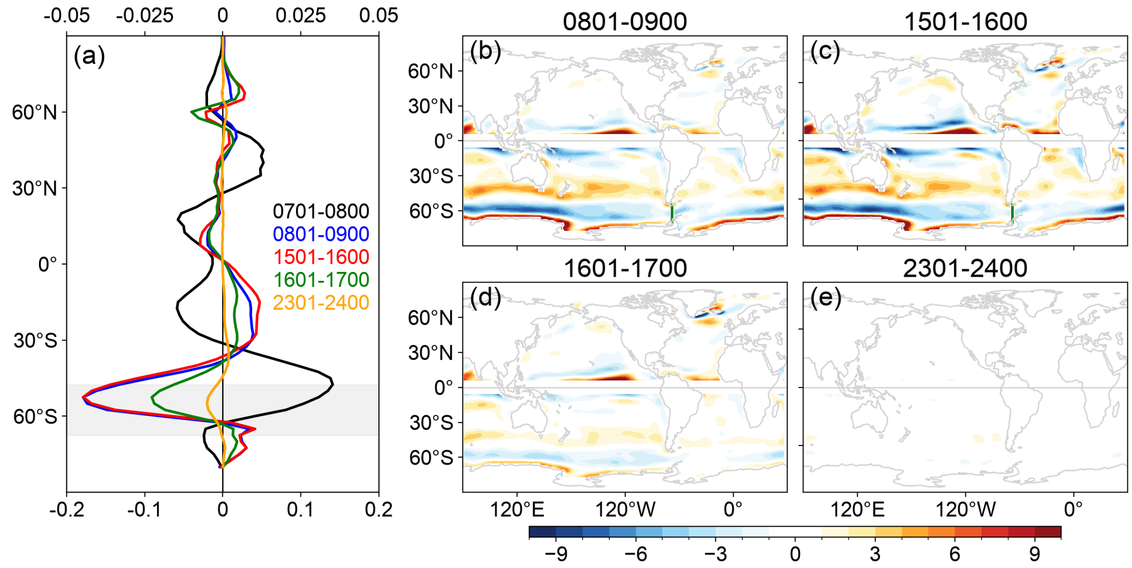

FIG. 6. Mean westerlies in Real (black curve; units: N m^{-2}; scale along the bottom abscissa) and changes in different years (units: N m^{-2}; scale along the top abscissa), with the years indicated in the figure. Changes in Ekman pumping (units: cm day^{-1}) in (b) 801–900, (c) 1501–1600, (d) 1601–1700, and (e) 2301–2400, respectively, with respect to 701–800. Positive (negative) values represent Ekman upwelling (downwelling).

The weakening of the Southern Hemisphere westerlies directly reduces wind-driven Ekman divergence and upwelling over much of the Southern Ocean (Figs. 6b, c). This response is dynamically important because Southern Ocean upwelling provides a major pathway through which deep waters, including NADW, return toward the surface and close the global overturning circulation. The reduced Ekman upwelling therefore acts together with the AABW-dominated abyssal circulation to restrict the Southern Ocean return pathway of NADW. Moreover, weaker upwelling reduces the supply of cold subsurface water to the surface around Antarctica, reinforcing the initial Antarctic warming and further weakening the meridional temperature gradient. The atmosphere–ocean response thus forms positive feedback in which Antarctic warming weakens the westerlies and Southern Ocean upwelling, while reduced upwelling in turn favors additional high-latitude warming.

Although Ekman pumping in the Southern Ocean is significantly weakened, Ekman pumping in the Antarctic marginal seas, including the Ross Sea, is enhanced (Figs. 6b–6d), which may be related to the reduction of winter sea ice cover in Antarctica (Fig. 5). However, other factors make the Ross Sea exhibit the clearest local dynamical response associated with enhanced AABW formation. Following DP closure, the anomalous high sea level pressure over the Ross Sea drives an anticyclonic surface wind anomaly (Figs. 7a1, a2), accompanied by elevated sea surface height (Figs. 7b1, b2) and enhanced convergence of the upper-ocean flow. At the same time, closure of the passage reorganizes the Southern Ocean barotropic circulation into a closed clockwise gyre (Figs. 7c1, c2). Relative to the open-DP state, poleward transport increases west of the passage, while the downstream flow turns westward along the Antarctic margin through the Bellingshausen and Ross Seas. This circulation pattern retains surface waters for longer within the cold Antarctic marginal seas and enhances their exposure to local wintertime buoyancy loss.

The atmospheric and oceanic circulation changes therefore act together to favor deep convection in the Ross Sea. The anticyclonic wind anomaly promotes local convergence and downwelling, while the reorganized gyre increases the residence time of surface waters within the AABW source region. Therefore, although Ekman pumping in the Ross Sea is enhanced, deep convection in the region is still greatly intensified. Consistent with this interpretation, the mixed layer deepens markedly in the Ross Sea after DP closure (Figs. 7d1, d2). The enhanced deep convection for AABW formation in these experiments is therefore concentrated primarily in the Ross Sea rather than the Weddell Sea, where altered surface buoyancy forcing, atmospheric circulation, and horizontal ocean advection reinforce one another.

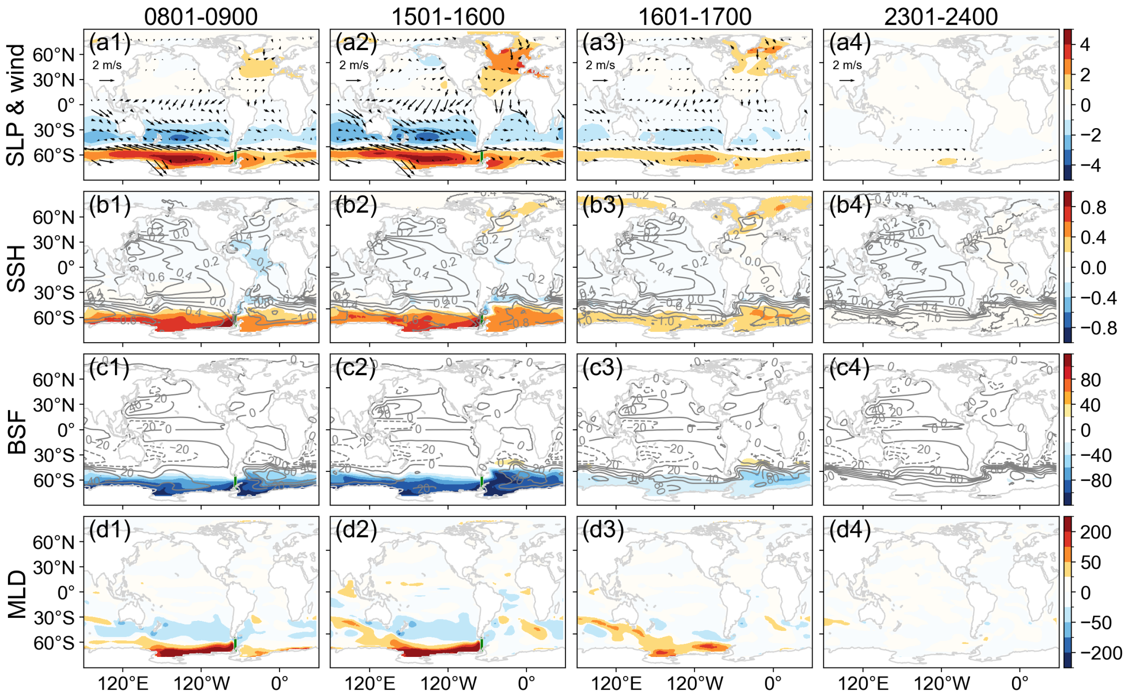

FIG. 7. Shading denotes changes in annual mean (a) sea level pressure (SLP; units: hPa) and surface wind, (b) sea surface height (SSH; units: m), (c) barotropic streamfunction (BSF; units: Sv), and (d) austral winter mixed layer depth (MLD; units: m) relative to the 701–800 mean, with the years indicated in the figure. In (b) and (c), contours denote the mean values for the corresponding years.

After the DP is reopened, the Southern Ocean circulation rapidly shifts back toward the open-gateway state. The ACC is reestablished (Figs. 7c3, c4), restoring the circumpolar pathway and reducing the anomalous poleward advection of warm, saline waters into the Antarctic marginal seas (Figs. 4a4–c4). The atmospheric circulation adjusts concurrently, with the Southern Hemisphere westerlies and sea level pressure pattern recovering toward their Real-state configurations (Figs. 6a, 7a3, a4). As a result, surface buoyancy forcing in the principal AABW source regions also returns toward its control-state distribution (Figs. 5c3, c4), while Ekman upwelling strengthens again across the Southern Ocean (Figs. 6d, e). These changes weaken AABW formation, reopen the Southern Ocean return pathway for NADW, and allow the AMOC to recover progressively (Fig. 1c). Consistent with the circulation response, the large-scale temperature, salinity, and density anomalies also decay toward their initial states (Fig. 3). The recovery therefore involves the coordinated reversal of the same Southern Ocean processes that drive the response to DP closure, although, as shown in Section 3, the individual components adjust on different timescales.

5. Conclusions and discussions

Using a fully coupled climate model, we have investigated how the AMOC responds to the closure and subsequent reopening of the DP. Closing the DP eliminates the unblocked circumpolar pathway and reorganizes both the atmospheric and oceanic circulations around Antarctica. Antarctic warming and sea-ice retreat modify surface buoyancy forcing in the AABW source regions, while the reduced meridional temperature gradient weakens the Southern Hemisphere westerlies and develops an anomalous anticyclonic circulation over the Ross Sea. This significantly weakens Southern Ocean Ekman upwelling and enhances downwelling and deep convection in the Ross Sea. These processes act together to enhance AABW formation through intensified deep convection in the Ross Sea. The resulting AABW-dominated abyssal circulation, combined with weakened wind-driven upwelling, strongly restricts the Southern Ocean return pathway of NADW. NADW formation consequently weakens and ultimately shuts down, leading to collapse of the NADW-dominated AMOC. Reopening the DP reverses these large-scale processes: the ACC and Southern Ocean upwelling recover, AABW weakens, the NADW return pathway is restored, and the AMOC is progressively reestablished.

The results highlight Southern Ocean ventilation as the key dynamical link between DP geometry and the AMOC. Two components are particularly important. The first is wind-driven Southern Ocean upwelling, which provides a major pathway for deep Atlantic waters to return toward the surface. The second is the AABW-associated abyssal circulation, which regulates the structure and accessibility of the deep return pathway. DP closure modifies both components simultaneously: weaker westerlies reduce Ekman upwelling from above, while stronger AABW reorganizes the abyssal circulation from below. Their combined effect isolates NADW from its principal Southern Ocean return route and favors an overturning state dominated by Antarctic deep-water formation. The adjustment is also strongly asymmetric in time. AABW formation and Southern Ocean overturning respond rapidly to changes in gateway geometry, whereas the NADW-dominated AMOC adjusts over several centuries. After reopening, Southern Ocean upwelling is restored before the AMOC fully recovers, indicating that reestablishment of the southern return pathway is necessary but not sufficient for the immediate recovery of NADW. Nevertheless, the overturning circulation ultimately returns close to its initial state, suggesting that the large-scale response to opposing DP perturbations is approximately reversible even though the transient pathways are not dynamically symmetric.

These results also have implications for the role of Southern Ocean gateways in the long-term evolution of the global meridional overturning circulation. Previous studies have emphasized the importance of the DP, Antarctic topography, atmospheric CO_2, sea ice, and paleogeography in shaping Cenozoic climate and ocean circulation (Sijp and England 2004, 2005; Zhang et al. 2010, 2011; Cristini et al. 2012; Lefebvre et al. 2012; Hutchinson et al. 2013; Toumoulin et al. 2020; Yang et al. 2024; Tong et al. 2025). Our results suggest that changes in DP geometry can influence the global overturning circulation not simply through the presence or absence of the ACC, but through a coupled reorganization of Southern Ocean buoyancy forcing, winds, AABW formation, and deep-water upwelling. However, the present experiments impose an idealized opening or closure of the DP under fixed preindustrial boundary conditions and therefore should not be interpreted as a direct reconstruction of the tectonic opening of the passage or of the Eocene–Oligocene transition. In the geological record, changes in gateway geometry occurred together with large changes in atmospheric CO_2, Antarctic ice sheets, and continental configuration. Proxy evidence further suggests that the transition from Pacific-dominated to Atlantic-dominated deep overturning occurred substantially later than the initial opening of the DP (Ferreira et al. 2018), indicating that gateway evolution alone cannot explain the establishment of the modern global overturning circulation. Quantifying how DP geometry interacts with Antarctic ice sheets, paleogeography, and changing climate boundary conditions therefore remains an important direction for future work.

Acknowledgements:

This research is jointly supported by the National Natural Science Foundation of China (Grant Nos. 42288101, 42230403, and 41725021) and by the Shanghai Frontiers Science Centre of Atmosphere–Ocean Interaction at Fudan University.

Data Availability Statement:

All data and code used in this study are available upon request.

Conflict of interest:

The authors have no relevant financial or non-financial interests to disclose.

REFERENCES

Baker, J. A., M. J. Bell, L. C. Jackson, G. K. Vallis, A. J. Watson, and R. A. Wood, 2025: Continued Atlantic overturning circulation even under climate extremes. *Nature*, **638**, 987–994, https://doi.org/10.1038/s41586-024-08544-0.

Beadling, R. L., J. L. Russell, R. J. Stouffer, P. J. Goodman, and M. Mazloff, 2019: Assessing the quality of Southern Ocean circulation in CMIP5 AOGCM and Earth system model simulations. *J. Climate*, **32**, 5915–5940, https://doi.org/10.1175/JCLI-D-19-0263.1.

Beadling, R. L., J. L. Russell, R. J. Stouffer, M. Mazloff, L. D. Talley, P. J. Goodman, J. B. Sallée, H. T. Hewitt, P. Hyder, and A. Pandde, 2020: Representation of Southern Ocean properties across Coupled Model Intercomparison Project generations: CMIP3 to CMIP6. *J. Climate*, **33**, 6555–6581, https://doi.org/10.1175/JCLI-D-19-0970.1.

Brady, E. C., and B. L. Otto-Bliesner, 2011: The role of meltwater-induced subsurface ocean warming in regulating the Atlantic meridional overturning circulation in glacial climate simulations. *Climate Dyn.*, **37**, 1517–1532, https://doi.org/10.1007/s00382-010-0925-9.

Broccoli, A. J., K. A. Dahl, and R. J. Stouffer, 2006: Response of the ITCZ to Northern Hemisphere cooling. *Geophys. Res. Lett.*, **33**, L01702, https://doi.org/10.1029/2005GL024546.

Cai, W., L. Gao, Y. Luo, X. Li, X. Zheng, X. Zhang, et al., 2023: Southern Ocean Warming and Its Climatic Impacts. *Sci. Bull.*, **68**, 946–960, https://doi.org/10.1016/j.scib.2023.03.049.

Chidichimo, M. P., K. A. Donohue, D. R. Watts, and K. L. Tracey, 2014: Baroclinic Transport Time Series of the Antarctic Circumpolar Current Measured in Drake Passage. *J. Phys. Oceanogr.*, **44**, 1829–1853, https://doi.org/10.1175/JPO-D-13-071.1.

Cristini, L., K. Grosfeld, M. Butzin, and G. Lohmann, 2012: Influence of the Opening of the Drake Passage on the Cenozoic Antarctic Ice Sheet: A Modeling Approach. *Palaeogeogr. Palaeoclimatol. Palaeoecol.*, **339–341**, 66–73, https://doi.org/10.1016/j.palaeo.2012.04.023.

DeConto, R. M., and D. Pollard, 2003: Rapid Cenozoic Glaciation of Antarctica Induced by Declining Atmospheric CO_2. *Nature*, **421**, 245–249, https://doi.org/10.1038/nature01290.

Donohue, K. A., K. L. Tracey, D. R. Watts, M. P. Chidichimo, and T. K. Chereskin, 2016: Mean Antarctic Circumpolar Current Transport Measured in Drake Passage. *Geophys. Res. Lett.*, **43**, 11760–11767, https://doi.org/10.1002/2016GL070319.

Elsworth, G., E. Galbraith, G. Halverson, et al., 2017: Enhanced weathering and CO_2 drawdown caused by latest Eocene strengthening of the Atlantic meridional overturning circulation. *Nat. Geosci.*, **10**, 213–216, https://doi.org/10.1038/ngeo2888.

England, M. H., D. K. Hutchinson, A. Santoso, and W. P. Sijp, 2017: Ice–Atmosphere Feedbacks Dominate the Response of the Climate System to Drake Passage Closure. *J. Climate*, **30**, 5775–5790, https://doi.org/10.1175/JCLI-D-15-0554.1.

Farneti, R., S. M. Downes, S. M. Griffies, S. J. Marsland, E. Behrens, M. Bentsen, et al., 2015: An assessment of Antarctic Circumpolar Current and Southern Ocean meridional overturning circulation during 1958–2007 in a suite of interannual CORE-II simulations. *Ocean Model.*, **93**, 84–120, https://doi.org/10.1016/j.ocemod.2015.07.009.

Ferreira, D., P. Cessi, H. K. Coxall, A. de Boer, H. A. Dijkstra, S. S. Drijfhout, et al., 2018: Atlantic–Pacific asymmetry in deep water formation. *Annu. Rev. Earth Planet. Sci.*, **46**, 327–352, https://doi.org/10.1146/annurev-earth-082517-010045.

Fyke, J. G., M. D'Orgeville, and A. J. Weaver, 2015: Drake Passage and Central American Seaway Controls on the Distribution of the Oceanic Carbon Reservoir. *Global Planet. Change*, **128**, 72–82, https://doi.org/10.1016/j.gloplacha.2015.02.011.

Gnanadesikan, A., 1999: A simple predictive model for the structure of the oceanic pycnocline. *Science*, **283**, 2077–2079, https://doi.org/10.1126/science.283.5410.2077.

Goldner, A., N. Herold, and M. Huber, 2014: Antarctic Glaciation Caused Ocean Circulation Changes at the Eocene–Oligocene Transition. *Nature*, **511**, 574–577, https://doi.org/10.1038/nature13597.

Gong, X., H. Liu, F. Wang, and C. Heuzé, 2022: On Atlantic Meridional Overturning Circulation in the CMIP6 Project. *Deep-Sea Res. II*, **206**, 105193, https://doi.org/10.1016/j.dsr2.2022.105193.

Gutierrez-Villanueva, M. O., T. K. Chereskin, and J. Sprintall, 2023: Compensating Transport Trends in the Drake Passage Frontal Regions Yield No Acceleration in Net Transport. *Nat. Commun.*, **14**, 7792, https://doi.org/10.1038/s41467-023-43499-2.

Han, Z., H. Yang, M. Tong, P. Wang, X. Hu, and S. Yang, 2026: Can the Drake Passage Affect the El Niño–Southern Oscillation Variability? *Ocean-Land-Atmos. Res.*, **5**, 0176, https://doi.org/10.34133/olar.0176.

Hill, D. J., A. M. Haywood, P. J. Valdes, et al., 2013: Paleogeographic Controls on the Onset of the Antarctic Circumpolar Current. *Geophys. Res. Lett.*, **40**, 5199–5204, https://doi.org/10.1002/grl.50941.

Hurrell, J. W., et al., 2013: The Community Earth System Model: A Framework for Collaborative Research. *Bull. Amer. Meteor. Soc.*, **94**, 1339–1360, https://doi.org/10.1175/BAMS-D-12-00121.1.

Hutchinson, D. K., M. H. England, A. Santoso, and A. McC. Hogg, 2013: Interhemispheric Asymmetry in Transient Global Warming: The Role of Drake Passage. *Geophys. Res. Lett.*, **40**, 1587–1593, https://doi.org/10.1002/grl.50341.

Hutchinson, D. K., A. M. de Boer, H. K. Coxall, R. Caballero, J. Nilsson, and M. Baatsen, 2018: Climate Sensitivity and Meridional Overturning Circulation in the Late Eocene Using GFDL CM2.1. *Clim. Past*, **14**, 789–810, https://doi.org/10.5194/cp-14-789-2018.

Jamieson, S. S. R., D. E. Sugden, and N. R. J. Hulton, 2010: The Evolution of the Subglacial Landscape of Antarctica. *Earth Planet. Sci. Lett.*, **293**, 1–27, https://doi.org/10.1016/j.epsl.2010.02.012.

Jamieson, S. S. R., N. Ross, G. J. G. Paxman, et al., 2023: An Ancient River Landscape Preserved Beneath the East Antarctic Ice Sheet. *Nat. Commun.*, **14**, 6507, https://doi.org/10.1038/s41467-023-42152-2.

Jiang, R., and H. Yang, 2021: Roles of the Rocky Mountains in the Atlantic and Pacific Meridional Overturning Circulations. *J. Climate*, **34**, 6691–6703, https://doi.org/10.1175/JCLI-D-20-0819.1.

Johnson, H. L., D. P. Marshall, and D. A. J. Sproson, 2007: Reconciling theories of a mechanically driven meridional overturning circulation with thermohaline forcing and multiple equilibria. *Climate Dyn.*, **29**, 821–836, https://doi.org/10.1007/s00382-007-0262-9.

Kennedy-Asser, A. T., D. J. Lunt, A. Farnsworth, et al., 2019: Assessing Mechanisms and Uncertainty in Modeled Climatic Change at the Eocene-Oligocene Transition. *Paleoceanogr. Paleoclimatol.*, **34**, 16–34, https://doi.org/10.1029/2018PA003380.

Kim, S.-Y., Y.-J. Choi, S.-W. Son, K. M. Grise, P. W. Staten, S.-I. An, et al., 2023: Hemispherically asymmetric Hadley cell response to CO_2 removal. *Sci. Adv.*, **9**, eadg1801, https://doi.org/10.1126/sciadv.adg1801.

Koenig, Z., C. Provost, R. Ferrari, N. Sennéchael, and M. Rio, 2014: Volume Transport of the Antarctic Circumpolar Current: Production and Validation of a 20 Year Long Time Series Obtained from In Situ and Satellite Observations. *J. Geophys. Res. Oceans*, **119**, 5407–5433, https://doi.org/10.1002/2014JC009966.

Kug, J.-S., J.-H. Oh, S.-I. An, S.-W. Yeh, S.-K. Min, S.-W. Son, et al., 2021: Hysteresis of the intertropical convergence zone to CO_2 forcing. *Nat. Clim. Change*, **12**, 47–53, https://doi.org/10.1038/s41558-021-01211-6.

Lagabrielle, Y., Y. Goddéris, Y. Donnadieu, J. Malavieille, and M. Suarez, 2009: The Tectonic History of Drake Passage and Its Possible Impacts on Global Climate. *Earth Planet. Sci. Lett.*, **279**, 197–211, https://doi.org/10.1016/j.epsl.2008.12.037.

Ladant, J.-B., Y. Donnadieu, L. Bopp, C. H. Lear, and P. A. Wilson, 2018: Meridional Contrasts in Productivity Changes Driven by the Opening of Drake Passage. *Paleoceanogr. Paleoclimatol.*, **33**, 302–317, https://doi.org/10.1002/2017PA003211.

Lefebvre, V., Y. Donnadieu, P. Sepulchre, D. Swingedouw, and Z. Zhang, 2012: Deciphering the Role of Southern Gateways and Carbon Dioxide on the Onset of the Antarctic Circumpolar Current. *Paleoceanography*, **27**, PA4201, https://doi.org/10.1029/2012pa002345.

Liu, W., and A. Hu, 2015: The role of the PMOC in modulating the deglacial shift of the ITCZ. *Climate Dyn.*, **45**, 3019–3034, https://doi.org/10.1007/s00382-015-2520-6.

Marshall, J., and F. Schott, 1999: Open-ocean convection: Observations, theory, and models. *Rev. Geophys.*, **37**, 1–64, https://doi.org/10.1029/98RG02739.

Marshall, J., and K. Speer, 2012: Closure of the meridional overturning circulation through Southern Ocean upwelling. *Nat. Geosci.*, **5**, 171–180, https://doi.org/10.1038/ngeo1391.

Mikolajewicz, U., E. Maier-Reimer, T. J. Crowley, and K. Kim, 1993: Effect of Drake and Panamanian Gateways on the Circulation of an Ocean Model. *Paleoceanography*, **8**, 409–426, https://doi.org/10.1029/93PA00893.

Munk, W. H., 1966: Abyssal recipes. *Deep-Sea Res. Oceanogr. Abstr.*, **13**, 707–730, https://doi.org/10.1016/0011-7471(66)90602-4.

Nakicenovic, N., and R. Swart, and Eds., 2000: *Emissions Scenarios*. Cambridge University Press, 570 pp.

Nong, G., R. Najjar, D. Seidov, and W. Peterson, 2000: Simulation of Ocean Temperature Change Due to the Opening of Drake Passage. *Geophys. Res. Lett.*, **27**, 2689–2692, https://doi.org/10.1029/1999GL011072.

Oh, J.-H., J.-S. Kug, S.-I. An, F.-F. Jin, M. J. McPhaden, and J. Shin, 2024: Emergent climate change patterns originating from deep ocean warming in climate mitigation scenarios. *Nat. Clim. Change*, **14**, 260–266, https://doi.org/10.1038/s41558-024-01928-0.

Orsi, A. H., G. C. Johnson, and J. L. Bullister, 1999: Circulation, mixing, and production of Antarctic Bottom Water. *Prog. Oceanogr.*, **43**, 55–109, https://doi.org/10.1016/S0079-6611(99)00004-X.

Pfister, P. L., T. F. Stocker, J. Rempfer, and S. P. Ritz, 2014: Influence of the Central American Seaway and Drake Passage on ocean circulation and neodymium isotopes: A model study. *Paleoceanography*, **29**, 1214–1237, https://doi.org/10.1002/2014PA002666.

Rahmstorf, S., 2002: Ocean circulation and climate during the past 120,000 years. *Nature*, **419**, 207–214, https://doi.org/10.1038/nature01090.

Russell, J. L., R. J. Stouffer, and K. W. Dixon, 2006: Intercomparison of the Southern Ocean circulations in IPCC coupled model control simulations. *J. Climate*, **19**, 4560–4575, https://doi.org/10.1175/JCLI3869.1.

Scher, H. D., and E. E. Martin, 2006: Timing and Climatic Consequences of the Opening of Drake Passage. *Science*, **312**, 428–430, https://doi.org/10.1126/science.1120044.

Sen Gupta, A., A. Santoso, A. S. Taschetto, C. C. Ummenhofer, J. Trevena, and M. H. England, 2009: Projected changes to the Southern Hemisphere ocean and sea ice in the IPCC AR4 climate models. *J. Climate*, **22**, 3047–3078, https://doi.org/10.1175/2008JCLI287.1.

Sijp, W. P., and M. H. England, 2004: Effect of the Drake Passage Throughflow on Global Climate. *J. Phys. Oceanogr.*, **34**, 1254–1266, https://doi.org/10.1175/1520-0485(2004)034<1254:EOTDPT>2.0.CO;2.

Sijp, W. P., and M. H. England, 2005: Role of the Drake Passage in Controlling the Stability of the Ocean's Thermohaline Circulation. *J. Climate*, **18**, 1957–1966, https://doi.org/10.1175/JCLI3376.1.

Sijp, W. P., and M. H. England, 2009: Atmospheric Moisture Transport Moderates Climatic Response to the Opening of Drake Passage. *J. Climate*, **22**, 2483–2493, https://doi.org/10.1175/2008JCLI2476.1.

Sijp, W. P., M. H. England, and J. R. Toggweiler, 2009: Effect of Ocean Gateway Changes under Greenhouse Warmth. *J. Climate*, **22**, 6639–6652, https://doi.org/10.1175/2009JCLI3003.1.

Sijp, W. P., M. H. England, and M. Huber, 2011: Effect of the Deepening of the Tasman Gateway on the Global Ocean. *Paleoceanography*, **26**, PA4207, https://doi.org/10.1029/2011PA002143.

Stommel, H., 1958: The abyssal circulation. *Deep-Sea Res.*, **5**, 80–82, https://doi.org/10.1016/S0146-6291(58)80014-4.

Stommel, H., 1961: Thermohaline convection with two stable regimes of flow. *Tellus*, **13**, 224–230, https://doi.org/10.3402/tellus.v13i2.9491.

Toggweiler, J. R., and B. Samuels, 1995: Effect of Drake Passage on the Global Thermohaline Circulation. *Deep-Sea Res. I*, **42**, 477–500, https://doi.org/10.1016/0967-0637(95)00012-U.

Toggweiler, J. R., and H. Bjornsson, 2000: Drake Passage and Palaeoclimate. *J. Quat. Sci.*, **15**, 319–328, https://doi.org/10.1002/1099-1417(200005)15:4<319::AID-JQS545>3.0.CO;2-C.

Tong, M., H. Yang, R. Jiang, and P. Wu, 2025: Pivotal Role of Tibetan Plateau and Antarctic in Shaping Present-Day Atlantic Meridional Overturning Circulation. *J. Climate*, **38**, 2239–2252, https://doi.org/10.1175/JCLI-D-24-0301.1.

Toumoulin, A., Y. Donnadieu, J.-B. Ladant, S. J. Batenburg, F. Poblete, and G. Dupont-Nivet, 2020: Quantifying the Effect of the Drake Passage Opening on the Eocene Ocean. *Paleoceanogr. Paleoclimatol.*, **35**, e2020PA003889, https://doi.org/10.1029/2020PA003889.

Tsujino, H., L. S. Urakawa, S. M. Griffies, G. Danabasoglu, A. J. Adcroft, A. E. Amaral, et al., 2020: Evaluation of global ocean–sea-ice model simulations based on the experimental protocols of the Ocean Model Intercomparison Project phase 2 (OMIP-2). *Geosci. Model Dev.*, **13**, 3643–3708, https://doi.org/10.5194/gmd-13-3643-2020.

Viebahn, J. P., A. S. von der Heydt, D. Le Bars, and H. A. Dijkstra, 2016: Effects of Drake Passage on a strongly eddying global ocean. *Paleoceanography*, **31**, 564–581, https://doi.org/10.1002/2015PA002888.

Wang, P., S. Yang, Z. Li, Z. Song, X. Li, and X. Hu, 2024: Role of the Antarctic Circumpolar Circulation in Current Asymmetric Arctic and Antarctic Warming. *Geophys. Res. Lett.*, **51**, e2024GL110265, https://doi.org/10.1029/2024GL110265.

Wang, P., Y. Han, X. Hu, Z. Li, X. Li, Y. Fang, J. Ying, and S. Yang, 2025: Impacts of Strengthened Antarctic Circumpolar Current on the Seasonality of Arctic Climate. *Geophys. Res. Lett.*, **52**, e2025GL115211, https://doi.org/10.1029/2025GL115211.

Watson, A. J., J. R. Ledwell, M.-J. Messias, B. A. King, N. Mackay, M. P. Meredith, B. Mills, and A. C. Naveira Garabato, 2013: Rapid cross-density ocean mixing at mid-depths in the Drake Passage measured by tracer release. *Nature*, **501**, 408–411, https://doi.org/10.1038/nature12432.

Weijer, W., W. Cheng, O. A. Garuba, A. Hu, and B. T. Nadiga, 2020: CMIP6 models predict significant 21st century decline of the Atlantic Meridional Overturning Circulation. *Geophys. Res. Lett.*, **47**, e2019GL086075, https://doi.org/10.1029/2019GL086075.

Wen, Q., and H. Yang, 2020: Investigating the Role of the Tibetan Plateau in the Formation of Pacific Meridional Overturning Circulation. *J. Climate*, **33**, 3603–3617, https://doi.org/10.1175/JCLI-D-19-0206.1.

Wen, Q., C. Zhu, Z. Han, Z. Liu, and H. Yang, 2021: Can the Tibetan Plateau affect the Antarctic Bottom Water? *Geophys. Res. Lett.*, **48**, e2021GL092448, https://doi.org/10.1029/2021GL092448.

Xu, X., E. P. Chassignet, Y. L. Firing, and K. Donohue, 2020: Antarctic Circumpolar Current Transport Through Drake Passage: What Can We Learn From Comparing High-Resolution Model Results to Observations? *J. Geophys. Res. Oceans*, **125**, e2020JC016365, https://doi.org/10.1029/2020JC016365.

Yang, H., and Q. Wen, 2020: Investigating the Role of the Tibetan Plateau in the Formation of Atlantic Meridional Overturning Circulation. *J. Climate*, **33**, 3585–3601, https://doi.org/10.1175/JCLI-D-19-0205.1.

Yang, H., R. Jiang, Q. Wen, Y. Liu, G. Wu, and J. Huang, 2024: The role of mountains in shaping the global meridional overturning circulation. *Nat. Commun.*, **15**, 2602, https://doi.org/10.1038/s41467-024-46856-x.

Yang, S., E. Galbraith, and J. Palter, 2014: Coupled Climate Impacts of the Drake Passage and the Panama Seaway. *Climate Dyn.*, **43**, 37–52, https://doi.org/10.1007/s00382-013-1809-6.

Zachos, J., M. Pagani, L. Sloan, E. Thomas, and K. Billups, 2001: Trends, Rhythms, and Aberrations in Global Climate 65 Ma to Present. *Science*, **292**, 686–693, https://doi.org/10.1126/science.1059412.

Zhang, Z., Q. Yan, and H. Wang, 2010: Has the Drake Passage Played an Essential Role in the Cenozoic Cooling? *Atmos. Oceanic Sci. Lett.*, **3**, 288–292, https://doi.org/10.1080/16742834.2010.11446884.

Zhang, Z., K. H. Nisancioglu, F. Flatøy, M. Bentsen, I. Bethke, and H. Wang, 2011: Tropical Seaways Played a More Important Role than High Latitude Seaways in Cenozoic Cooling. *Clim. Past*, **7**, 801–813, https://doi.org/10.5194/cp-7-801-2011.